Final Report for AOARD Grant FA2386-12-1-4078 "Development of Pulsating Tubules with Chiral Inversion"

Date 2013-09-21

PI and Co-PI information: Myongsoo Lee; myongslee@snu.ac.kr; Seoul National University; Department of Chemistry; Seoul National University, Gwanak-ro 1, Gwanak-gu, Seoul 151-747, Korea; 82-2-880-4340; 82-2-393-6096.

Period of Performance: 08/16/2012 – 08/15/2013

Abstract: Stimuli responsive nanostructures through rigid-flexible block molecules can hold a great promise for the fabrication of intelligent nanodevices, nanoelectronics, and nanobiomaterials. One of the typical features of the rod amphiphiles is its unique anisotropic molecular shape and strong aggregation tendency through additional π–π stacking interactions, which have enabled the construction of highly versatile and dynamic nanostructures. Hence, variations in the molecular structure and the local environment, albeit small, allow the rapid transformation of equilibrium morphology. In this project, we have studied the development of stimuli-responsive nanomaterials using on self-assembly of amphiphilic molecules based on hydrophilic oligo(ethylene glycol) chains and hydrophobic aromatic rods and peptides.

Introduction: Supramolecular nanostructures produced via self-assembling molecules have attracted interest because the sophisticated structures formed by weak noncovalent interactions can be triggered by external stimuli leading to dynamic materials. Typical examples of basic building blocks for self-assembly include lipid molecules, surfactants, supra-amphiphiles, block molecules, hyperbranched polymers, peptide derivatives and inorganic/organic complexes. Among them, rigid-flexible block molecules, consisting of aromatic rod and coil segments, are promising candidates for fabricating self-assembled structures. Aqueous assemblies have great advantages for the creation of desired materials in terms of biological applications. For the aqueous self-assembly of amphiphilic rigid-flexible block molecules, the anisotropic orientation of the stiff rod-like segments and the microsegregation of the incompatible molecular parts are able to enhance each other in water leading to the formation of thermodynamically stable supramolecular structures with a rigid hydrophobic core surrounded by flexible hydrophilic chains. In general, monodisperse rod–coil blocks display highly reproducible and predictable self-assembly behavior.

Recently, we have studied on the development of diverse aqueous assemblies, such as tubules, toroids, porous capsules, and helical fibers, by adjusting the relative volume fraction between hydrophobic and hydrophilic segments of rod–coil molecules consisting of aromatic units and poly(propylene oxide) (PPO) or poly(ethylene oxide) (PEO) coils. In this project, we focus on the development of aqueous nanostructure from the self-assembly of rod–coil block molecules. We also demonstrated the self-assembly of α-helical peptide. Finally, we showed the application of self-assembled nanostructures into biological system.

Part 1: Supramolecular Switching between Flat Sheets and Helical Tubules Triggered by Coordination Interaction.

Experiment : We envisioned that the introduction of meta-linked pyridine units at both ends of

Report Documentation Page

Form Approved
OMB No. 0704-0188

1. REPORT DATE	2. REPORT TYPE	3. DATES COVERED
15 OCT 2013	**Final**	**16-08-2012 to 15-08-2013**

4. TITLE AND SUBTITLE
Development of Pulsating Tubules from Non-Covalent Macrocycles

5a. CONTRACT NUMBER
FA23861214078

5b. GRANT NUMBER

5c. PROGRAM ELEMENT NUMBER

6. AUTHOR(S)
Myong Soo Lee

5d. PROJECT NUMBER

5e. TASK NUMBER

5f. WORK UNIT NUMBER

7. PERFORMING ORGANIZATION NAME(S) AND ADDRESS(ES)
Seoul National University,Seoul,151-747,Seoul,KR,151747

8. PERFORMING ORGANIZATION REPORT NUMBER
N/A

9. SPONSORING/MONITORING AGENCY NAME(S) AND ADDRESS(ES)
AOARD, UNIT 45002, APO, AP, 96338-5002

10. SPONSOR/MONITOR'S ACRONYM(S)
AOARD

11. SPONSOR/MONITOR'S REPORT NUMBER(S)
AOARD-124078

12. DISTRIBUTION/AVAILABILITY STATEMENT
Approved for public release; distribution unlimited

13. SUPPLEMENTARY NOTES

14. ABSTRACT

Stimuli responsive nanostructures constructed from rigid-flexible block molecules hold great promise for fabrication of intelligent nanodevices, nanoelectronics, and nanobiomaterials. One typical feature of rod amphiphiles is their unique anisotropic molecular shape and strong aggregation tendency through π−π stacking interactions, which has enabled construction of highly versatile and dynamic nanostructures. Variations in molecular structure and local environment, albeit small, allow the rapid transformation of equilibrium morphology. This research project involved development of stimuli-responsive nanomaterials using self-assembly of amphiphilic molecules based on hydrophilic oligo(ethylene glycol) chains and hydrophobic aromatic rods and peptides. Pyridine end-substituted rod?coil block systems were found to self-assemble into flat sheets in dilute aqueous solution, but through reversible coordination interaction with Ag+1 could change their shape into helical tubules at higher and discrete macrocycles at lower concentrations. Metal-containing macrocycles were found to reversibly stack to form helical tubules in response to variation in concentration. The influence of interactions with small molecule planer aromatics on 2D structure was examined. Rationally designed macrobicyclic amphiphiles consisting of a hydrophilic dendron attached to the center of an aromatic plane undergoes self-assembly into a 2D structure with nanosized lateral pores through lateral association of amphiphile dimers with a uniform diameter of 3.5 nm. The porous sheets efficiently intercalate flat aromatic molecules, such as coronene, through the conformational inversion of the basal planes of the dimeric micelles. This project also examined a novel approach to make short peptides adopt stable α-helical structures through macrocyclization of their linear precursors. On incorporation of more hydrophobic amino acid residues into the peptide block, the helical structure forces the cyclic molecules to adopt a facially amphiphilic conformation resulting in amphiphilic folding of the cyclic molecule and to formation of undulated nanofibers through directional assembly of discrete micelles. Controlling conformation and stability of the nanofibers tethered by lectin proteins were found to regulate T cell activation. The lengths as well as stability of the protein-coated supramolecular nanofibers could be manipulated by a small variation in the rod?coil molecular structure. The unique supramolecular structures with switchable functionality reported herein might provide new strategies for the design of intelligent materials with simultaneous biological and electro-optical functions.

15. SUBJECT TERMS

Self-Assembly, Stimuli-Responsive Materials, Tubular Nanostructures, Dynamic Response, 2D Nanostructures, Proteins, T-Cells, Nanofibers.

16. SECURITY CLASSIFICATION OF:			17. LIMITATION OF ABSTRACT	18. NUMBER OF PAGES	19a. NAME OF RESPONSIBLE PERSON
a. REPORT	b. ABSTRACT	c. THIS PAGE			
unclassified	**unclassified**	**unclassified**	**Same as Report (SAR)**	**13**	

the bent-shaped aromatic segment might form stimuli-responsive 2D structures, since pyridine units are well-known to interact specifically with Ag(I) ions through reversible coordination bonds. This recognition event would cause reversible rearrangement of the fully overlapped zigzag packing arrangement of the bent-shaped rigid segments to maximize the coordination interactions between pyridine donors and Ag(I) ions at the expense of π–π stacking interactions between aromatic rod segments. Consequently, this metal-directed rearrangement of the aromatic segments would endow the 2D structures with dynamic responsive functions. With this direction of research in mind, we synthesized self-assembling molecules 1 and 2 consisting of a long bent-shaped aromatic segment containing *m*-pyridine units at both ends and a hydrophilic oligoether dendron with an S configuration grafted at the apex. Here we report their spontaneous self-assembly to form responsive 2D sheets in aqueous solution (Figure 1). Notably, these 2D sheets reversibly transform into hollow tubules with helical cavities through a cyclic conformation of the aromatic segments in response to Ag(I) ions (see Figure 5). The aromatic amphiphiles were synthesized starting with Suzuki coupling of a 2,6-dibromophenol derivative with trimethylsilyl (TMS)-protected phenylboronic acid. The resulting compound was subjected to an etherification reaction with an oligoether dendritic chain. The transformation of the TMS groups to iodo groups was achieved by iodination with ICl. Suzuki couplings of the diiodo compound with TMS-substituted biphenylboronoic acid and TMS-substituted phenylboronic acid were used to prepare the precursors of 1 and 2, respectively. The final compounds were successfully synthesized by Suzuki coupling with 3-pyridylboronic acid. The resulting molecules were characterized by ^{1}H and ^{13}C NMR spectroscopies and MALDI-TOF mass spectroscopy and shown to be in full agreement with the structures presented.

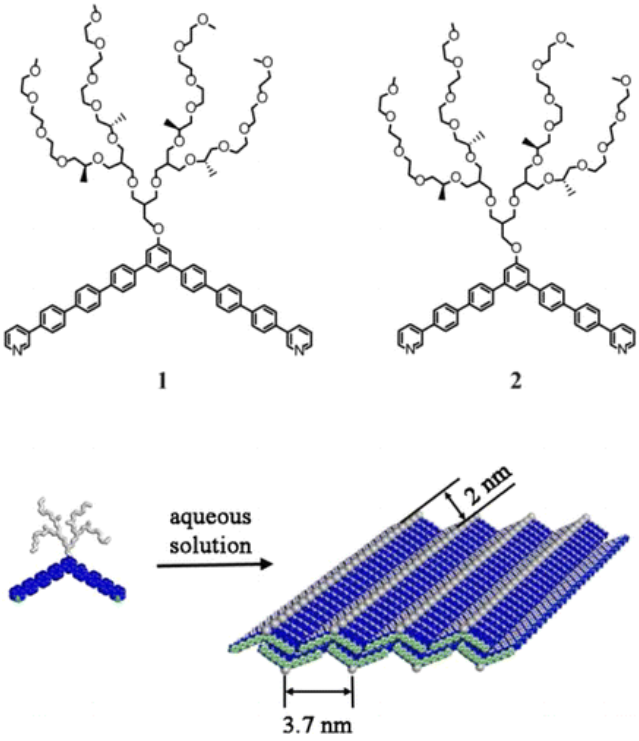

Figure 1. Molecular structures of bent-shaped amphiphiles 1 and 2 and schematic representation of the formation of responsive 2D sheets

Results and Discussion : Molecule 1 self-assembles into flat sheets in dilute aqueous solutions. Cryogenic transmission electron microscopy (cryo-TEM) showed sheetlike objects with curved edges against the vitrified solution background (Figure 2a), indicative of the formation of flexible sheets in bulk solution. To obtain more information on these sheets, we additionally performed TEM experiments with samples cast onto a TEM grid and negatively stained with uranyl acetate. The image shows planar sheets with regular stripes having a periodicity of 2 nm against a dark background (Figure 2b inset). This result suggests that the aromatic segments with a zigzag conformation are oriented parallel to the sheet plane, similar to the organization in the layered structures of bent-shaped molecules. The interapex distance of 3.7 nm within the zigzag conformation, as obtained from molecular modeling, indicates that the adjacent aromatic segments are slipped relative to each other with an angle of 57.4° to release the steric hindrance between the bulky dendritic chains (Figure 1).

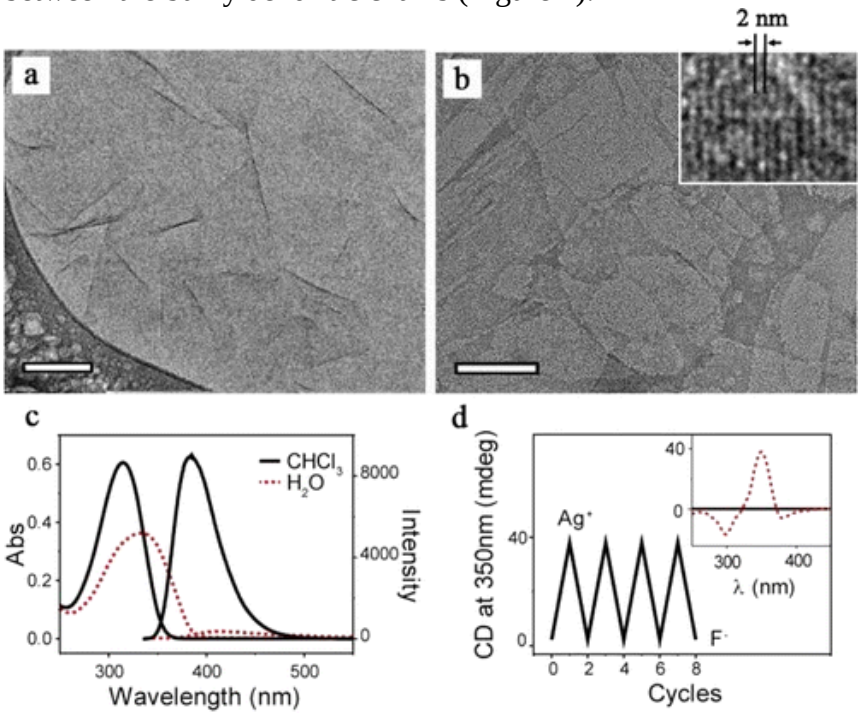

Figure 2. (a) Cryo-TEM image and (b) negative-stain TEM image of 1 obtained from a 0.03 wt % aqueous solution (scale bars = 100 nm). The inset is a magnified image of (b). (c) Absorption and emission spectra of 1 (0.03 wt %) in CHCl3 solution (solid black lines) and aqueous solution (dotted red lines); λ_{ex} = 315 and 333 nm, respectively. (d) Reversible CD signal changes at λ_{max} = 350 nm for an aqueous solution of 1 (0.03 wt %) upon cycles of complexation and subsequent decomplexation. The inset shows CD spectra of an aqueous solution of 1 (0.03 wt %) without Ag(I) ions (solid black line) and with Ag(I) ions (dotted red line).

Optical spectroscopy investigation of 1 displayed that the absorption maximum in aqueous solution is red-shifted and the fluorescence intensity significantly quenched with respect to those observed in chloroform solutions, indicative of the formation of aqueous aggregates through π–π interactions of the aromatic segments (Figure 2c).(3a, 11) When molecule 1 in aqueous solution was subjected to circular dichroism (CD) measurements, no CD signals could be detected, as would be expected for symmetric 2D objects, even though 1 contains chiral side groups (Figure 2d). To investigate the effect of the length of the aromatic segments for the 2D sheets, we also

investigated 2, an analogue of 1 with shorter aromatic segments. In great contrast to 1, 2 did not show any aggregation behavior in aqueous solution even at high concentrations.

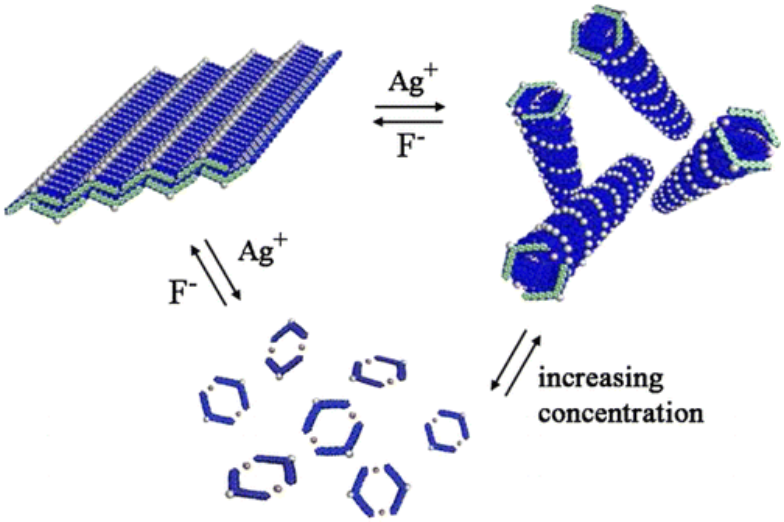

Figure 3. Schematic representation of reversible transformation through flat sheets, helical tubules and discrete toroids in response to external stimuli.

The sheets can be considered to undergo a drastic transformation into helical tubules at a higher concentration and a transformation into discrete dimeric macrocycles at a lower concentration through reversible coordination interactions between the pyridine units of the aromatic segments and Ag(I) ions (Figure 3). Another interesting point to be noted is that the metal-containing macrocycles reversibly stack on top of each other to form helical tubules in response to a variation in the concentration. The primary driving force responsible for the metal-directed switching behavior of the sheets is the dominant coordination interactions between the pyridine units of the aromatic segments and Ag(I) ions, which overcome the weak stacking interactions of the aromatic segments. This interplay of different non-covalent interactions allows the 2D structures to be transformed immediately into helical or macrocyclic structures depending on the concentration.

In conclusion, we have demonstrated that stimuli-responsive 2D structures can be constructed by the aqueous self-assembly of bent-shaped aromatic rods containing pyridine units at their terminals. The sheets respond to Ag(I) ions by changing their shape into helical tubules at a higher concentration and discrete macrocycles at a lower concentration. It is worth noting that the metal-containing macrocycles reversibly stack on top of each other to form helical tubules in response to the variation in concentration. In comparison with conventional fixed 2D structures, the most notable feature of our systems is their ability to respond to external stimuli by a direct structural change from nonchiral flat 2D structures to 1D hollow structures with helical pores. Such a unique switch of the open sheets into closed tubules with helical pores opens up the new possibility of using the 2D structures to capture specific proteins selectively in their helical interior and release them to their target.

Part 2: Directional Assembly of α-Helical Peptides Induced by Cyclization.

Experiment : Many important biological functions originate from molecular recognition events

of proteins. For many proteins to bind various biomolecules, well-defined secondary structures are placed in the recognition domains. The α-helix is a common motif in the secondary structure of proteins, especially existing vastly in the recognition domains of various protein–protein or nucleic acid–protein interactions. Inspired by biological systems, many studies have been focused on the development of stable α-helixes to mimic the interactions between the original proteins. However, folding of short peptides into an α-helical structure in solution is limited because stabilizing interactions and the enthalpy gain from hydrogen bonds between amides on adjacent helical turns are not sufficient to compensate for the entropic cost involved in the folding of the peptide chain.

Herein we report a novel approach to make short peptides adopt a stable α-helical structure through macrocyclization of their linear precursors. When more hydrophobic amino acid residues are incorporated into the peptide block, the helical structure forces the cyclic molecules to adopt a facially amphiphilic conformation (Figure 1b). The resulting amphiphilic folding of the cyclic molecule leads to the formation of undulated nanofibers through directional assembly of discrete micelles.

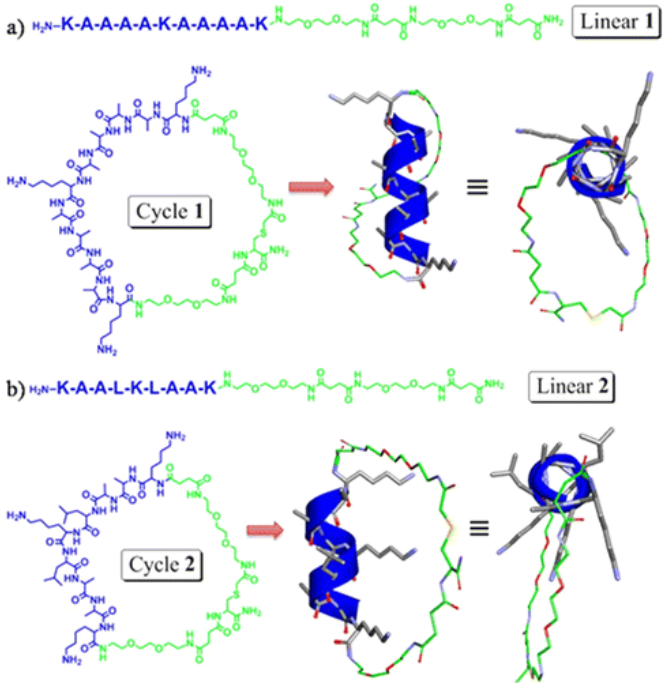

Figure 1. Molecular structures of cyclic and linear peptides and schematic illustrations of α-helical structures: (a) KAAAAKAAAAK sequence; (b) KAALKLAAK sequence.

We synthesized small cyclic diblock molecules composed of a peptide and a flexible linker. Cycle 1 as a model compound for the molecular-level helix stabilization is based on a (KAAAA)n repeat sequence, which has been reported to form a monomeric helix in aqueous solution. A perpendicular view of the peptide helix axis (Figure 1a) shows that three amino residues from lysine side chains are equally spaced to minimize the electrostatic repulsion between the amino groups, resulting the same polarity around the helix surface. The effect of molecular cyclization was examined by comparing linear 1 and cycle 1, which are composed of the short peptide segment KAAAAKAAAAK and a flexible linker. In addition to the stabilization of the monomeric small peptide helix, we designed cycle 2 based on the sequence that can form a facially amphiphilic helix (Figure 1b). Cycle 2 has a KAALKLAAK sequence, and the three amino groups in the molecule are placed in the same face of the helix when the

helical structure is formed. Moreover, the leucine residues, which are known to interact with each other through hydrophobic interactions, can be utilized to provide a hydrophobic surface on one side of the helix. The facial amphiphilicity of this design is easily seen in the view from the perpendicular helix axis (Figure 1b). An ethylene glycol-based linker segment, N-(Fmoc-8-amino-3,6-dioxaoctyl)succinamic acid, was introduced as a flexible linker unit. The cyclization reaction was performed with an on-resin cyclization method to achieve high synthetic efficiency. Each molecule was characterized by MALDI mass spectroscopy.

Results and Discussion : We investigated the peptide secondary structures of cycle 1 and linear 1 to confirm the effect of macrocyclization on α-helix stabilization using circular dichroism (CD) spectroscopy in the universally used electrolyte condition, aqueous KF solution, and pure water (Figure 2a). An α-helix was successfully formed in cycle 1, in contrast to the completely random coil structure of its linear counterpart. In the CD spectra, cycle 1 showed negative bands at 204 and 222 nm and a positive band at 190 nm, indicative of a typical α-helix. Dangling amide bonds at the linker position that adopts a free conformation would contribute a little amount to the deviation from the perfect helix band (208 nm negative band). It should be noted that the CD signals remained unaltered upon heating to 60 °C, indicating that the helical structure is stable within our experimental temperature range. In great contrast, the linear 1 peptide showed a typical random coil structure with a strong negative band at 196 nm and no signals at 222 nm. Figure 2b shows CD spectra comparing the helix stabilization effect of the cyclization with that of the well-known helix-stabilizing agent TFE (30% solution). Indeed, the peak intensity at 222 nm that is indicative of helicity is larger for the cyclic system than for the TFE-stabilized linear peptide system, indicating that the helix stabilization effect in the cyclic system is even greater than that of TFE. These results demonstrate that the cyclization is an effective method for stabilizing small α-helixes in a monomeric fashion in typical aqueous salt solutions. This result can be explained by considering the confinement of the peptide segment to a cyclic structure, in which its entropy penalty is much less because of its constrained nature. The degree of freedom of the cyclic peptide chain is much reduced compared with its linear peptide chain, resulting in the achievement of an enthalpically favorable helix conformation.

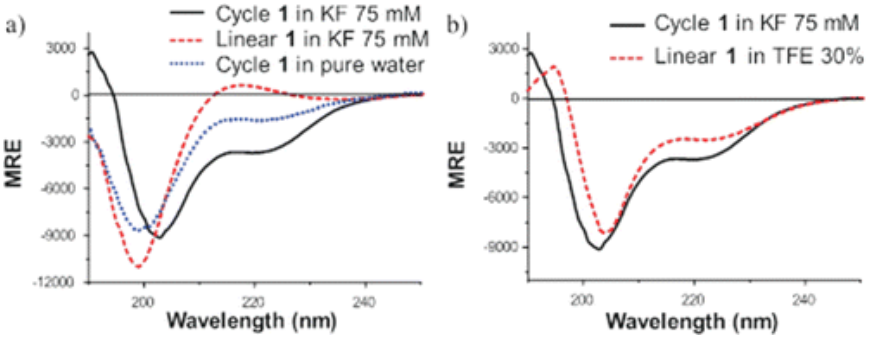

Figure 2. CD spectra of cyclic and linear peptides: (a) cycle 1 and linear 1 in 75 mM aqueous KF solution (black solid and red dashed lines, respectively) and cycle 1 in pure water (blue dotted line); (b) cycle 1 in 75 mM aqueous KF solution (black solid line) and linear 1 in 30% TFE (red dashed line).

Because this system is based on a peptide and a hydrophilic flexible coil segment, amphiphilic characteristics could be induced by incorporating more hydrophobic residues into the peptide segment. With this in mind, we investigated whether the cycle 2 molecule would form a helical

structure to induce an amphiphilic feature. Similar to cycle 1, cycle 2 also adopted a helical conformation different from its linear counterpart (Figure 3a). This was rather surprising because the three amino groups in cycle 2 are even more closely spaced in the helix. In contrast to its linear counterpart, which did not show apparent aggregation behavior, the cyclic peptide self-assembled into a fibrous structure while maintaining an α-helical conformation of the hydrophobic peptide unit. The transmission electron microscopy (TEM) image (Figure 3c) shows the formation of unique nanofibers with regular undulation along the fiber axis that have diameters of 6–7 nm and lengths of a few hundred nanometers. Closer examination of the samples showed the individual objects along the fiber axis to be oblate rather than spherical (Figure 3c inset), suggesting that the undulation arises from the micellar stacking.

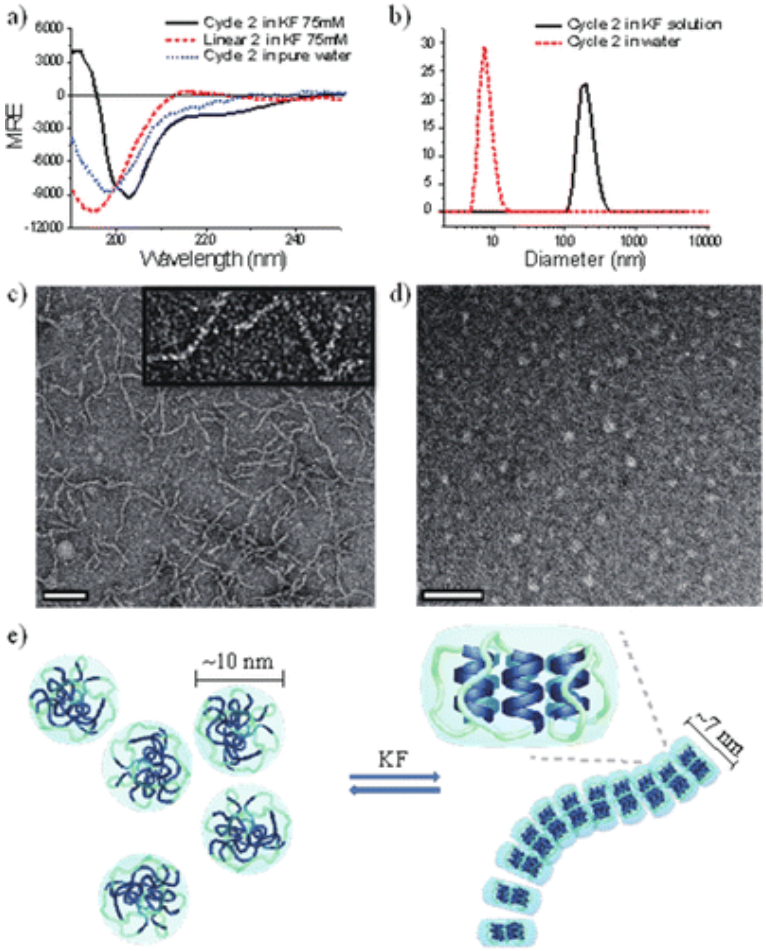

Figure 3. (a) CD spectra of the peptides based on KAALKLAAK sequence: cycle 2 and linear 2 in 75 mM aqueous KF solution (black solid and red dashed lines, respectively) and cycle 2 in pure water (blue dotted line). (b) Size distribution graph from DLS measurements of aqueous solution: cycle 2 in KF solution (black solid line) and cycle 2 in water without salt (red dashed line). (c, d) Negative-stain TEM images of cycle 2 in (c) KF solution and (d) pure water (scale bars = 100 nm). (e) Schematic representation of the transformation between micelles and undulated nanofibers.

To gain insight into the mechanism for the formation of the undulated nanofibers, we investigated the aggregation behavior in pure water without any electrolytes. Interestingly, the CD signal drastically shifted toward lower wavelengths (Figure 3a), indicating that the helical structure of the peptide segments was transformed predominantly into a random coil

conformation. This conformational change was accompanied by a structural transformation from the elongated fibers to spherical micelles. Dynamic light scattering (DLS) analysis showed a drastic reduction in the hydrodynamic diameter from several hundred nanometers to 10 nm upon removal of KF salt (Figure 3b). The TEM image shows spherical micelles with an average diameter of 10 nm, which is larger than the fiber width (Figure 3d). These results suggest that the leucine–leucine interactions are destabilized in a random coil conformation, resulting in looser packing between the peptide segments in pure water than in KF solution. Consequently, the looser packing of the hydrophobic peptide segments with a random coil conformation gives rise to the spherical micelles with a larger diameter than the fiber width.

From these observations, induction of the α-helical structure of the peptide segment seems to be the main driving force for the formation of the undulated nanofibers. In the KF solution, which provides a more hydrophobic environment because of the salting-out effect, peptide chains would favor being folded into α-helixes. The general effect of salting out in helix stabilization was observed from cycle 1 folding upon removal of the KF salt (Figure 2a). The helicity of the peptide decreased, as determined from the size of 222 nm band and the much-shifted negative minimum. With aid of this salting-out effect, the resulting helical peptides, cycle 2, are oriented parallel to each other to form oblate micelles in which the hydrophobic leucine residues are located on the inside and lysine units together with the hydrophilic linkers are on the exterior. This anisotropic packing arrangement of the helical peptides results in oblate micelles with more hydrophobic tops and bottoms resulting from the α-helical core. To reduce the exposure of the hydrophobic parts of the micelles in a water environment, the oblate micelles stack on top of each other to form undulated nanofibers (Figure 3e).

In conclusion, we have demonstrated that cyclization of block peptides leads to a conformational transition of the peptide segment from random coil to α-helix, which is important for many biological applications of small epitopes. When amphiphilicity was introduced into our cyclic system by elaborate modification of the peptide sequence, the helical conformation of the peptide forced the molecular cycle to be facially amphiphilic. The resulting facial amphiphiles self-aggregated into unique undulated nanofibers originating from one-dimensional stacking of oblate micelles through directional interactions.

Part 3: Switchable Nanoporous Sheets by the Aqueous Self-Assembly of Aromatic Macrobicycles

Experiment : The self-assembling molecules that form this aggregate consist of a macrobicyclic aromatic segment and a hydrophilic oligoether dendron grafted at the center of the basal plane (Figure 1). The synthesis of the flat aromatic amphiphiles began with the Sonogashira coupling of a dendron-substituted diiodobenzene derivative with 2,6-dibromoethynylbenzene to provide a tetrabromo building block (see the Supporting Information). Suzuki coupling of the tetrabromo compound with 3-((triisopropylsilyl)ethynyl)phenylboronic acid ester, followed by silyl-group deprotection with tetra-*n*-butylammonium fluoride, then provided a precursor with four terminal alkyne groups. The final aromatic amphiphiles were synthesized efficiently by intramolecular Glaser-type coupling of the terminal alkyne groups under dilute reaction conditions (CuCl/CuCl2 in pyridine).9 The resulting molecules were characterized by ^{1}H and ^{13}C NMR spectroscopy and MALDI-TOF mass spectrometry and were shown to be in full agreement with the structures presented.

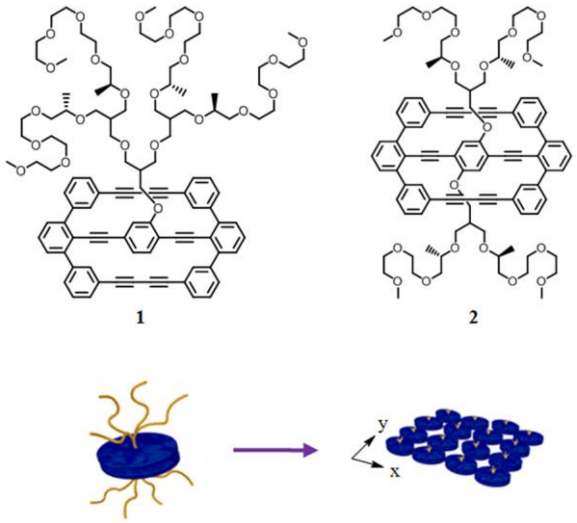

Molecule 1 self-assembles into nanoporous sheets in dilute aqueous solutions. Cryogenic transmission electron microscopy (cryo-TEM) showed sheetlike objects with curved edges against the vitrified solution background (Figure 2 a); this observation is indicative of the formation of flexible sheets in bulk solution. Notably, a high-resolution image revealed that the sheets contained in-plane nanopores with an average diameter of approximately 4 nm (Figure 2 a, inset). To obtain more information on these sheets, we also performed TEM experiments with the samples cast onto a TEM grid (and negatively stained with uranyl acetate). A low-magnification image showed planar sheets with rugged surfaces against a dark background. A higher-magnification image showed that the rugged surfaces consisted of uniform micelles and nanopores (Figure 2 b, inset) and thus suggested that the sheets had formed through a lateral association of small, discrete micelles. The diameters of the micelles and the pores were measured to be approximately 3.5 nm and 3–5 nm, respectively. The micellar diameter is about twice the length of the molecule and thus indicates the presence of dimeric micelles with a face-to-face stacking of the aromatic basal planes. Further apparent evidence for the formation of in-plane dimeric micelles was provided by topochemical polymerization of the sheets. Polymerization of the diacetylene groups by irradiation of the solution with UV light for 6 h yielded only dimers. This result demonstrates that the primary structure of the 2D sheets consists of dimeric micelles in which the two aromatic planes within the micellar core face one another in a slipped π–π stack for efficient dimerization of the diacetylene groups.

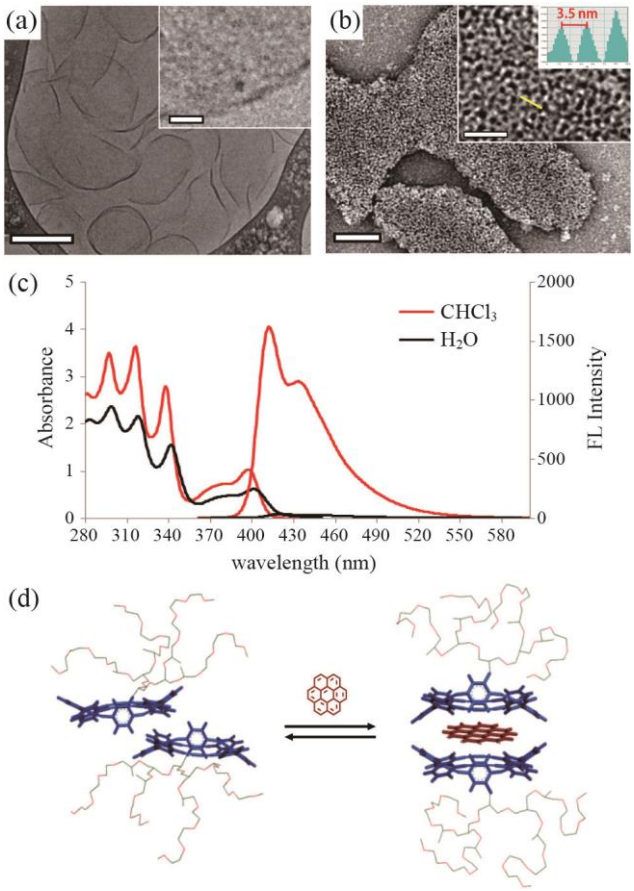

Figure 2. a) Cryo-TEM image of a solution of 1 (200 μm; scale bar: 200 nm). b) Negatively stained TEM image of nanoporous sheets from a 100 μm aqueous solution of 1 (scale bar: 100 nm). The insets in (a) and (b) show magnified images (scale bars: 20 nm) and the line scan profile along the yellow line. c) Absorption and emission spectra of 1 (100 μm) in $CHCl_3$ (red line) and aqueous solution (black line); λ_{ex}=318 nm. d) Molecular modeling of the dimeric micelle without coronene and the dimeric micelle containing coronene.

The formation of 2D sheets based on pairs of face-to-face-stacked aromatic molecules stimulated us to investigate whether the planar nanostructure would encapsulate flat aromatic guest molecules, such as coronene, through π–π stacking interactions in aqueous solution (Figure 2 d). Indeed, the 2D sheets readily solubilized coronene in aqueous solution with preservation of their 2D structure. Upon the addition of coronene to an aqueous solution of 1, the fluorescence intensity at 530 nm associated with the coronene emission increased until 0.5 equivalents of coronene had been added. Upon the further addition of coronene to the solution, the fluorescence intensity did not change, and precipitation was observed. Therefore, it can be concluded that the maximum coronene loading per amphiphilic molecule is 0.5 equivalents. This result implies that the flat conjugated aromatic guest is sandwiched between the two aromatic basal planes of the dimeric micelles through hydrophobic and π–π stacking interactions. Atomic force microscopy (AFM) images showed that the layer thickness increased from 2.1 to 2.5 nm upon the addition of coronene (Figure 3 a,b). Thus, it appears that the coronene molecules, which have a flat conjugated surface, are effectively intercalated between the aromatic planes of the dimeric micelles.

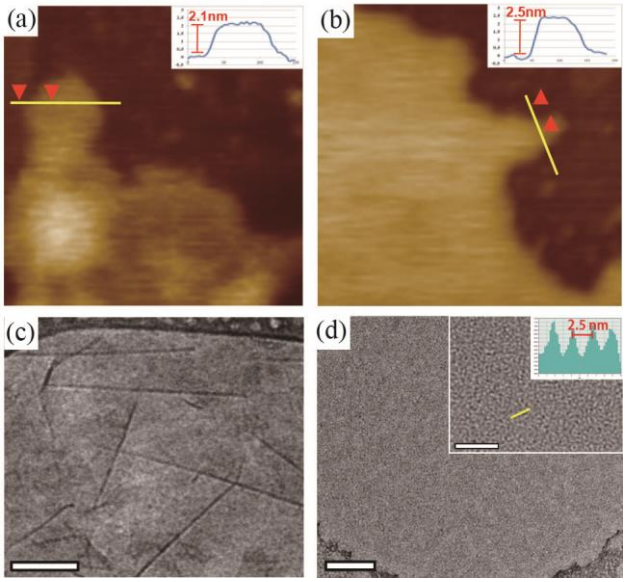

Figure 3. a,b) AFM images of 1 (a) and 1–coronene (b; 50 μm aqueous solution, 700×700 nm^2) and cross-sectional analysis of the images. c) Cryo-TEM image of a 100 μm aqueous solution of 1–coronene (scale bar: 100 nm). d) Negatively stained TEM image of closed sheets from a 100 μm aqueous solution of 1–coronene (scale bar: 100 nm). The inset shows a magnified image (scale bar: 20 nm) and the line profile along the yellow line.

We investigated the influence of coronene intercalation on the 2D structure by cryo-TEM analysis of a solution of 1 in the presence of coronene (0.5 equiv; Figure 3 c). The resulting image shows large planar sheets with straight edges and thus indicates that the flexible sheets become stiff upon the intercalation of coronene and that the 2D structure is preserved. Notably, a TEM image of a cast film negatively stained with uranyl acetate shows large sheets with smoothly embossed surfaces without any noticeable nanopores (Figure 3 d). This image shows that the lateral pores are closed upon the addition of coronene guest molecules. The magnified image shows that the diameter of the in-plane micelles decreases from 3.5 to 2.5 nm upon the addition of coronene (Figure 2 b, inset and Figure 3 d, inset; see also Figure S5) and thus indicates that the intercalation of the aromatic guests causes the in-plane micelles to become laterally more closely packed.

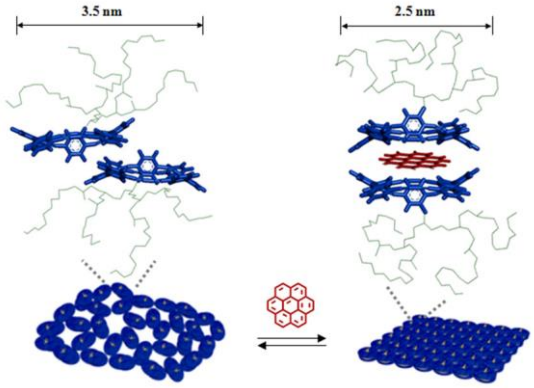

Figure 4. Schematic representation of the switch between a nanoporous sheet and a closed sheet, as triggered by the intercalation of coronene.

In conclusion, we have demonstrated that a rationally designed macrobicyclic amphiphile

consisting of a hydrophilic dendron attached to the center of an aromatic plane undergoes self-assembly into a 2D structure with nanosized lateral pores through the lateral association of amphiphile dimers with a uniform diameter of 3.5 nm. The porous sheets efficiently intercalate flat aromatic molecules, such as coronene, through the conformational inversion of the basal planes of the dimeric micelles. Notably, the intercalation of a flat conjugated aromatic guest causes the reversible transformation of the porous sheets into closed sheets without sacrificing the 2D structure. This switch is also accompanied by change in the flexibility of the self-assembled 2D structure from a flexible to a rigid state. This unique supramolecular structure with switchable functionality might provide a new strategy for the design of intelligent materials with simultaneous biological and electrooptical functions. In particular, the reversible switching of the pores opens up the possibility of pumping molecules of interest out of the internal pores of such 2D systems.

Part 4. Protein-coated nanofibers for promotion of T cell activity.

Experiment : We have reported that carbohydrate-functionalized multivalent ligands could be constructed by the self-assembly of rod–coil block molecules. These supramolecular ligands agglutinated effectively specific bacterial cells through carbohydrate-mediated multivalent interactions. Here, we describe protein-coated nanofibers that regulate T cell activities via multivalent interactions. The molecules that form the bioactive nanofibers consist of a laterally grafted rod–coil molecular architecture containing hydrophilic carbohydrate segments which can bind to a lectin protein, Con A (Figure 1). The synthesis of laterally grafted rod amphiphiles 1 and 2 has been reported in a previous study. These molecules self-assembled into elongated fiber-like objects in aqueous solution, which is consistent with the reported result (Figure 2a and b).

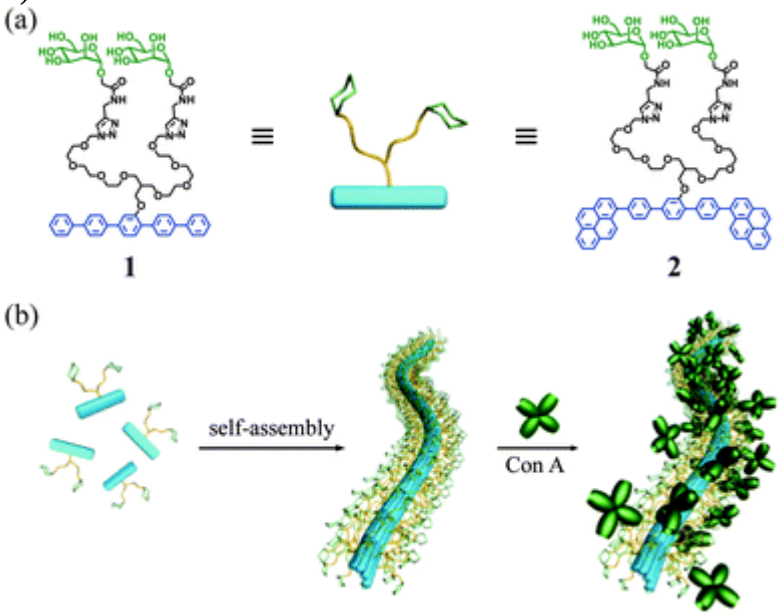

Figure 1. (a) The chemical structure of amphiphiles 1 and 2. (b) Representation of protein-coated nanofibers.

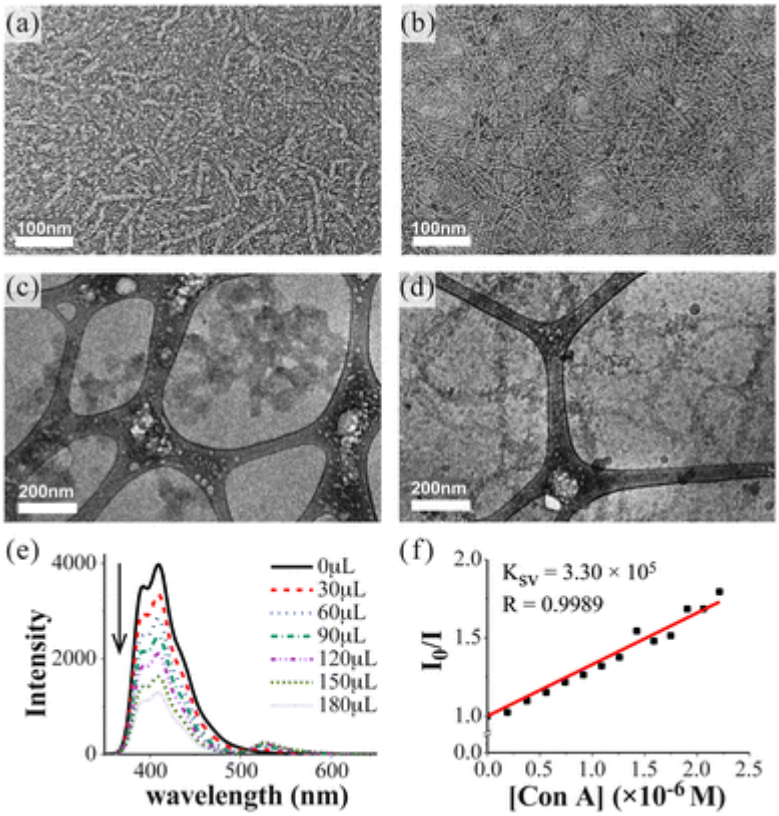

Figure 2. TEM images of (a) short fibers of 1 and (b) long fibers of 2 in aqueous solution. Cryo-TEM images of (c) an irregular assembly of 1 with Con A, and (d) Con A-coated nanofibers of 2. The results of FRET experiments upon the addition of fluorescein-labeled Con A (2 mg per mL), respectively, to a solution containing amphiphile 1; (e) the whole fluorescence spectra and (f) a Stern–Volmer plot of the fluorescence signal, λ_{ex} = 409 nm.

The negatively stained sample of 1 showed the formation of short nanofibers with lengths of 100–200 nm and a width of around 8 nm. While molecule 2 containing pyrene units at both ends of ter(*p*-phenylene) aggregated into much longer nanofibers than molecule 1, with a uniform width of around 6 nm and a length of over 2 μm (Fig. 2b). Because the pyrene units triggered a stronger π–π stacking interaction between aromatic segments than the simple oligophenylene unit, 2 could self-assemble into extended nanofibers with enhanced conformational stability rather than 1. These nanofibers consisting of hydrophilic exterior with a high density of mannose units are able to function as multivalent ligands binding lectin protein, Con A. To investigate the multivalent interactions of the nanofibers, we have added Con A (2 mg per mL, 0.2 equiv. of mannose residues) into the solutions of 1 and 2 (1.2 mM mannose residues), respectively, resulting in Con A-tethered nanofibers. Cryogenic transmission electron microscopy (cyro-TEM) revealed that 1 formed irregular aggregates with the addition of Con A, indicating that the nanofibers of 1 are not stable in a Con A solution. The strong carbohydrate–protein interactions of 1 seemed to frustrate the weak self-assembly of loosely packed penta-p-phenylene units of the molecule. In great contrast, the nanofibers of 2 showed an unchanged fibrillar shape even after the addition of Con A. Cryo-TEM images of 2 with Con A revealed that the length of the fibers is several micrometers with a thickness of 40 nm. Considering that the size of Con A is 10 nm, this dimension of the thickness indicates that the nanofibers are coated with lectin proteins on their exterior while maintaining their fibrillar structures. This result demonstrates that the packing arrangements of the aromatic segments based on the pyrene units within internal cores

play a critical role in forming protein-tethered stable nanostructures.

Fluorescence resonance energy transfer (FRET) could provide one of the good methods to monitor the formation of soluble Con A–ligand complexes. Subsequently, FRET experiments were carried out with the mixtures of fluorescein-labeled Con A and amphiphiles 1 and 2, respectively. As the amount of labeled Con A in a solution containing amphiphile 1 increased, the intensity of fluorescence emission associated with the pentaphenylene segments decreased (Fig. 2e). Similar to 1, 2 also showed the fluorescence quenching of the aromatic segments upon the addition of the fluorescein-labeled Con A. On the basis of the fluorescence titration spectra, the Stern–Volmer constants (K_{sv}) of amphiphiles 1 and 2 by Con A were found to be 3.30 × 105 and 3.72 × 105, respectively, predominantly through static quenching (Figure 2). It demonstrated that the binding affinity was not significantly different between each sample with Con A. This result indicates that the carbohydrate ligands effectively bind Con A through specific ligand–protein interactions

Results and Discussion : Con A-coated nanofibers are expected to bind T cell surfaces through multivalent interactions between the carbohydrates on the cell surfaces and multivalent lectin proteins to activate T cells. Along this line, the effect of supramolecular multivalent protein nanofibers on live T cells was evaluated using ELISA assay for the induction of interleukin 2 (IL-2) in the Jurkat cells (human T lymphocyte). Upon the treatment of Con A and Con A-coated nanostructures, the Jurkat cells were activated and released IL-2. Con A could induce intracellular signal transduction and cause Jurkat cells to release 100 to 300 times as much IL-2 as lectin-stimulated normal human peripheral blood lymphocytes. In our experiment, Jurkat cells (1.0 × 105 per mL) were incubated with a preincubated solution of mannose-functionalized nanofibers and Con A at 37 °C and 5% CO_2. In the cytotoxicity test, the value of viability is not significantly different between each sample, demonstrating that Con A-tethered nanostructures are cytocompatible without sacrificing cell viability (Figure 3a). The activation of mitogen-stimulated T cells can be measured by secreted IL-2 after 2 to 4 hours and mainly occurs during the first 48 hours. After 24 hours of cell culture, cell media were harvested and were used for the test in the IL-2 ELISA assay. Figure 3b shows that the in the premixed solution of 2 and Con A there is increased production of IL-2, approximately 80% than Con A alone. In the case of 1 and Con A, however, the amount of IL-2 secretion displays similar values to the mannose fiber of 2 without Con A, indicating no activation of T cells. This result suggests the enhanced binding affinity of multivalent Con A-coated nanofibers which can surround more receptors on the cell surface than other extracellular materials. The extended and long nanofibers formed from the self-assembly of amphiphile 2 could induce stronger Con A–receptor multivalent interactions for receptors clustering than Con A tetramers alone (Figure 3c and e).

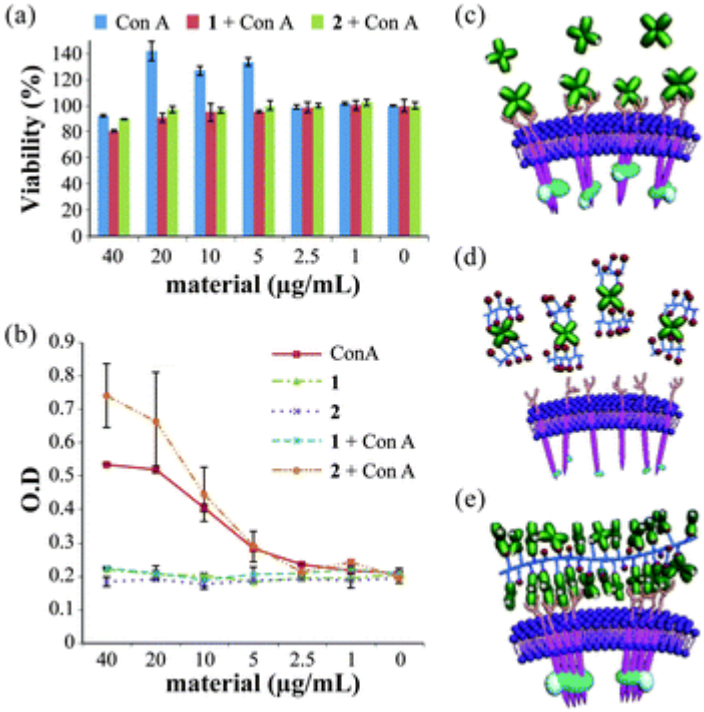

Figure 3. (a) The viability test using the water-soluble tetrazolium salt (WST) method of Jurkat cells grown with Con A, 1 + Con A and 2 + Con A for one day. (b) Comparison of IL-2 production by Con A and scaffolded Con A. The error bars in (a) and (b) indicate the standard deviations from three experiments performed in duplicate, and some are smaller than the symbols. Schematic representation of IL-2 production depending on the fiber length. (c) Con A alone, (d) 1 + Con A and (e) 2 + Con A.

In summary, we have demonstrated that controlling the conformation and stability of the nanofibers tethered by lectin proteins can regulate T cell activation. The lengths as well as stability of the protein-coated supramolecular nanofibers could be manipulated by a small variation in the rod–coil molecular structure. Elongated nanofibers with stronger aromatic interactions maintained their fibrillar shape even after tethering Con A, which was not possible with the short and weakly assembled nanofibers. Notably, extended and long multivalent ligands promote T cell activation compared with monovalent Con A ligands, observed by the secretion of IL-2 and the fluorescence emission. These long and flexible supramolecular multivalent architectures could arrange the desired receptors regularly and be adapted to the mobile cytoskeleton simultaneously. A self-assembled multivalent architecture based on aromatic rod–dendritic coil can offer many opportunities for developing biocompatible and bio-responsive systems.

List of Publications and Significant Collaborations that resulted from your AOARD supported project:

1) Shin, S.; Lim, S.; Kim, Y.; Kim, T.; Choi, T. L.; Lee, M.: Supramolecular switching between flat sheets and helical tubules triggered by coordination interaction. *J. Am. Chem. Soc.*, **2013**, *135*, 2156-2159.

2) Sim, S.; Kim, Y.; Kim, T.; Lim, S.; Lee, M.: Directional assembly of alpha-helical peptides induced by cyclization. *J. Am. Chem. Soc.*, **2012**, *134*, 20270-20272.

3) Kim, Y.; Shin, S.; Kim, T.; Lee, D.; Seok, C.; Lee, M.: Switchable nanoporous sheets by the aqueous self-assembly of aromatic macrobicycles. *Angew. Chem. Int. Ed.* **2013**, *52*, 6426-6429.

4) Kim, T.; Lee, H.; Kim, Y.; Nam, J. M.; Lee, M.: Protein-coated nanofibers for promotion of T cell activity. *Chem. Commun*. **2013**, *49*, 3949-3951.

5) Kim, Y.; Li, W.; Shin, S.; Lee, M.: Development of Toroidal Nanostructures by Self-Assembly: Rational Designs and Applications. *Acc. Chem. Res.*, **2013**, *ASAP*.

6) Li, W.; Kim, Y.; Lee, M.: Intelligent supramolecular assembly of aromatic block molecules in aqueous solution. *Nanoscale* **2013**, *5*, 7711-7723.

7) Kim, Y.; Kim, T.; Lee, M.: From self-assembled toroids to dynamic nanotubules. *Polymer Chemistry* **2013**, *4*, 1300-1308.